

## Ultraviolet camera measurements of passive and explosive (strombolian) sulphur dioxide emissions at Yasur volcano, Vanuatu

Ilanko, T.<sup>1</sup>, Pering, T.D.<sup>1\*</sup>, Wilkes, T.C.<sup>1</sup>, Woitischek, J.<sup>2,3</sup>, D'Aleo, R.<sup>4</sup>, Aiuppa, A.<sup>5</sup>, McGonigle, A.J.S.<sup>1,6,7</sup>, Edmonds, M.<sup>2</sup>, Garaebaeti, E.<sup>8</sup>

<sup>1</sup> Department of Geography, University of Sheffield, Winter Street, Sheffield, S10 2TN, UK

<sup>2</sup> Department of Earth Sciences, University of Cambridge, Downing Street, Cambridge, CB2 3EN, UK

<sup>3</sup> BPI Institute, BP Institute, University of Cambridge, Madingley Rd, CB3 0EZ, UK

<sup>4</sup> INGV, Sezione di Palermo, Via Ugo la Malfa 153, 90146, Palermo, Italy

<sup>5</sup> DiSTeM, Università di Palermo, Via Archirafi, 22, 90123 Palermo, Italy

<sup>6</sup> School of Geosciences, the University of Sydney, NSW2006, Australia

<sup>7</sup> Faculty of Health, Engineering and Sciences, University of Southern Queensland, Toowoomba, QLD 4350, Australia

<sup>8</sup> Geohazards Division, Vanuatu Meteorology and Geo-hazards Department, Lini Highway, Port Vila, Vanuatu

\*Corresponding author: [t.pering@sheffield.ac.uk](mailto:t.pering@sheffield.ac.uk)

### Abstract

Here, we present the first ultraviolet (UV) camera measurements of sulphur dioxide (SO<sub>2</sub>) flux from Yasur volcano, Vanuatu, for the period 6<sup>th</sup> – 9<sup>th</sup> July 2018 and the first direct gas based measurements of explosive gas masses from this target. Yasur typically exhibits persistent passive gas release interspersed with frequent strombolian explosions. We used the ‘PiCam’ Raspberry Pi UV Camera system (Wilkes et al., 2017, 2016) engineered in a more compact format and powered through solar panels. Our daily median SO<sub>2</sub> fluxes range 4.0-5.1 kg s<sup>-1</sup>, with a measurement uncertainty of -12.2% to +14.7%, including errors from: gas cell calibration drift, uncertainties in plume direction and distance, as well as plume velocity. This work highlights the use of particle image velocimetry (PIV) for plume velocity determination, which was deemed to be more preferable than the typically used cross-correlation and optical flow methods, because of the ability to function over a range of plume conditions. We calculate SO<sub>2</sub> masses for strombolian explosions of 8 to 81 kg (mean of 32 kg), to our knowledge the first budget of explosive gas masses from this target, and through the use of a simple statistical measure using the moving minimum, we estimate that passive degassing is the dominant mode of gas emission at Yasur, supplying an average of ~69% of the total gas released. Our work serves to further highlight the utility of UV camera measurements in volcanology and, in particular, the benefit of the multiple camera approach in error characterisation. This work also adds to our inventory of gas-based data to characterise the spectrum of strombolian activity across the globe, concerning Yasur which previously has received relatively little attention in terms of released gas fluxes.

## Highlights

- Long time series data collected using portable solar chargeable UV cameras.
- Particle image velocimetry (PIV) used for plume velocity measurements.
- SO<sub>2</sub> fluxes daily median values of 4.0-5.1 kg s<sup>-1</sup>.
- SO<sub>2</sub> masses produced by strombolian explosions range 8 to 81 kg (mean 32 kg).

## 1. Introduction

Strombolian volcanism is one of the more common forms of basaltic explosive activity globally, associated with the rapid ejection of hot pyroclasts from a vent in a single impulsive burst (Blackburn et al., 1976; Taddeucci et al., 2015), with event frequencies ranging from seconds to minutes (Pering and McGonigle, 2018). Volcanoes with frequent strombolian activity include: the archetypal Stromboli, Italy (Patrick et al., 2007; Ripepe et al., 2002); Pacaya, Guatemala (Battaglia et al., 2018; Dalton et al., 2010); Erebus, Antarctica (Ilanko et al., 2015; Johnson and Aster, 2005; Oppenheimer et al., 2009; Sweeney et al., 2008); and Yasur, Vanutu (Bani and Lardy, 2007; Kremers et al., 2013; Oppenheimer et al., 2006), the subject of this study. Other volcanoes also known to produce strombolian activity include: Etna, Italy (Aiuppa et al., 2016; Branca and Del Carlo, 2005; Pering et al., 2015) Villarrica, Chile (Shinohara and Witter, 2005); Arenal, Costa Rica (Garcés et al., 1998; Szramek et al., 2006); Batu Tara, Indonesia (Gaudin et al., 2017a; Laiolo et al., 2018); and Shishaldin, USA (Vergnolle et al., 2004).

Classically, this style of behaviour has been related to the ascent from depth of elongated and over-pressured bubbles, which rapidly expand in length as they approach the surface, termed gas slugs (Taylor bubbles) (Del Bello et al., 2012; James et al., 2008; Seyfried and Freundt, 2000; Taddeucci et al., 2015). However, recent research has suggested that the causal driving mechanisms may be far more diverse (Barth et al., 2019; Suckale et al., 2016; Woitischek et al., 2020), and that the presence of crystal-rich layers in the magmatic column is important in the formation of strombolian explosions. To test these hypotheses, it is useful to investigate the spectrum of strombolian activity at targets, including Yasur, where this behaviour is typical. In addition, recent studies have highlighted the importance of eruption frequency in determining the behaviour of ascending gas slugs (Gaudin et al., 2017a) as well as inter-slug interactions (Pering et al., 2017, 2015). This has led to a classification of behaviour styles ranging from rapidly bursting slugs which may interact with one another during ascent, through to single bursting slugs, where interactions do not apply (Pering et al., 2017; Pering and McGonigle, 2018).

There are several instrumental means to obtain information about individual strombolian explosions, which are based on capture of: seismic (Chouet et al., 2003; Ripepe et al., 2002), infrasonic (Dalton et al., 2010; Delle Donne et al., 2016; Johnson and Ripepe, 2011; Marchetti et al., 2009), thermal (Patrick et al., 2007; Ripepe et al., 2002), and gas-derived (McGonigle et al., 2009; Pering et al., 2015; Pering et al., 2016; Tamburello et al., 2012) data. Here, we focus on gas emission rate measurements, using the ultraviolet (UV) camera, a frequently used technique for constraining gas release from persistently outgassing volcanoes (McGonigle et

al., 2017; Pering et al., 2019a). The UV camera is able to resolve rapid fluctuations in the release of sulphur dioxide (SO<sub>2</sub>) gas, and when it is used in tandem with a multi-component gas analyser (Multi-GAS), which measures gas ratios when placed inside a volcanic plume (Aiuppa et al., 2005; Shinohara et al., 2015), it is possible to estimate the total gas emission rate (Pering et al., 2014). An important parameter in respect of generation mechanisms for strombolian explosions is the relative proportions of gas released during explosions to that released passively (Barth et al., 2019; Jaupart and Vergnolle, 1988, 1989; Parfitt, 2004; Suckale et al., 2016; Vergnolle and Jaupart, 1986). This ‘active’ to passive degassing ratio also provides information about conduit fluid dynamics (Gaudin et al., 2017a, 2017b; Pering et al., 2015; Pering et al., 2016). For example, Tamburello et al., (2012) discovered that the most efficient mode of degassing at Stromboli was actually the passive degassing, supplying ~77% of gases released, demonstrating the continued importance of passive gas release (Carn et al., 2017) and the smaller gas bubbles within a volcanic conduit.

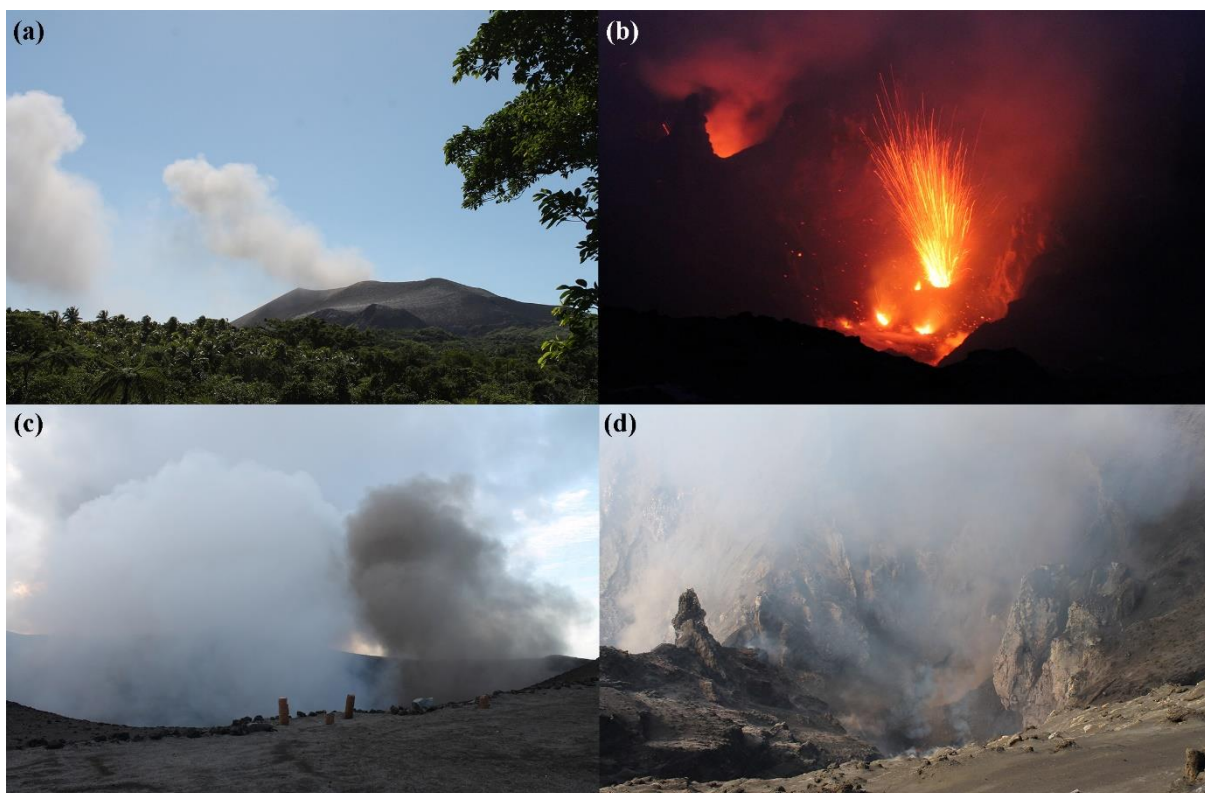


**Figure 1:** Activity at Yasur Volcano, Vanuatu, during the July 2018 field campaign. (a) Image of the gas plume rising from the summit crater. Large gas pulses are associated with explosions; (b) a night-time view with the south crater in the foreground and incandescence from the north crater in the background. Several vents are visible in the south crater with one sourcing a strombolian explosion; (c) ash-rich gas plumes formed by strombolian explosions occurred from the north crater and ash-poor gas plumes from explosions from the south crater; (d) a day-time view into the north crater, showing the crater floor topography divided by a septum into northern and southern craters.

UV camera derived SO<sub>2</sub> masses from strombolian explosions (Delle Donne et al., 2016; Mori and Burton, 2009; Pering et al., 2015; Tamburello et al., 2012) can also be combined with gas

ratio data (e.g., from Multi-GAS), to generate total gas masses and volumes for individual explosive events (Burton et al., 2007; Pering et al., 2016). These overall mass data can then be used to parameterise analytical and computational models for gas flow in conduits, to glean further information about the activity and generating mechanisms, for example, pertaining to slug length, explosive vigour, and categorisation of burst behaviour using fluid dynamics (Del Bello et al., 2012; James et al., 2009, 2008; Pering and McGonigle, 2018).

Here we demonstrate the use of a portable, solar-chargeable, version of the low-cost Raspberry Pi ultraviolet camera (Wilkes et al., 2017, 2016) combined with a new approach to estimate plume velocity using UV camera imagery to obtain SO<sub>2</sub> fluxes. We present the first UV camera measurements at Yasur, providing the first gas-based estimate of explosive strombolian gas masses, key to unravelling information on the spectrum of behaviours on this style of activity globally. Furthermore, we illustrate the use of statistical methods to differentiate between passive and explosive gas release, and finally apply mathematical models to estimate driving slug dimensions of the strombolian explosions at Yasur volcano.

## ***2. Yasur volcano and eruptive and degassing activity during 5<sup>th</sup>-11<sup>th</sup> July 2018***

Yasur (Vanuatu) is a basaltic stratovolcano located on the southeast of Tanna Island, which is thought to have been predominantly persistently active for at least ~800 years (Firth et al., 2014). The main volcanic edifice is a cone with a crater area of 350-450 m diameter, divided by a septum into northern and southern craters, each containing multiple active vents. During the field campaign measurement period an ashy plume was present throughout the week, related to ash-rich strombolian explosions arising from both craters (Fig 1). From the summit, multiple vents displaying incandescence were visible within the southern crater, each of which exhibited different styles of explosive behaviour. Gas release from the summit vents was constantly visible, occasionally including ‘puffing’ behaviour (described elsewhere by Gaudin et al., 2017b, 2017a; Pering and McGonigle, 2018; Tamburello et al., 2012). The northern crater contained at least two vents, but access to this crater’s rim was prevented on the grounds of safety due to ballistic ejecta from the crater’s strombolian explosions, which appeared to be more ash-rich than those from the southern crater. From the southern crater we directly observed explosions from at least three vents, each of which had different behaviours, two with jet-like characteristics (i.e., with a strong vertical component to the ejecta vector), highlighting the potential for interaction with the conduit wall during the explosion process, i.e., the explosion (slug burst) happens within the conduit, providing a vertical steer to the released material (Delle Donne and Ripepe, 2012; Salvatore et al., 2020). Another vent exhibited parabolic transport of incandescent pyroclasts (without initial jet), as though an ascending bubble burst within an over-topped magma column (Del Bello et al., 2012), or within a flared conduit geometry (Dibble et al., 2008), i.e., allowing the lateral expansion of bubble prior to burst. Interestingly these observations of strombolian explosions also had clearly differentiable audible properties, with the non-jet-like explosions associated with a deeper booming sound. During 8 – 9 July, explosions were frequently associated with visible shockwaves propagating through the condensed plume. The supplementary video highlights a snapshot of typical activity captured from the both craters. Throughout the measurement period, the morphology

of the crater was dynamic, with spatter and ash accumulating around vents leading to changes in the size, shape, and position of vents.

A number of studies on Yasur have focused on the characteristics of strombolian activity and, in particular, its dynamism. Multi-vent basaltic volcanoes are known to exhibit vent-specific behaviours which can change through time, e.g., Salvatore et al. (2018) concerning Stromboli. Simons et al., (2020) discuss systematic changes in behaviour at individual vents within the southern crater at Yasur, with switching from bomb-rich (incandescent pyroclasts) through to ash-rich explosions. They also discuss conduit branching and the possibility of a common source bubble (i.e., gas slug) driving paired explosions from separate vents at Yasur, with the potential for diverging eruption styles at the vents being linked to cooling of the magma in the upper conduit sections. La Spina et al., (2016) observed two decoupled styles of degassing from infrasound data: puffing, which was observed as near-constant; and strombolian explosions. Meier et al., (2016) highlighted the ash-rich and ash-poor (or bomb-rich), respectively styles and their similarity at Yasur to those of Stromboli (Gaudin et al., 2014b; Patrick et al., 2007; Ripepe et al., 2005; Ripepe and Marchetti, 2002; Taddeucci et al., 2012). Kremers et al. (2013) were able to calculate the lengths of gas slugs generating the strombolian explosions on Yasur, ranging from 59 to 244 m, with mean and median values of 112 m and 103 m, respectively.

SO<sub>2</sub> fluxes at Yasur ranged from 2.5 to 17.2 kg s<sup>-1</sup> from April 2004 to November 2005, with a mean of 7.9 kg s<sup>-1</sup> based on differential optical absorption spectroscopy (DOAS) traverses (Bani and Lardy, 2007). Between August 2007 and December 2008, SO<sub>2</sub> fluxes at Yasur were 1.3 to 11.1 kg s<sup>-1</sup>, with a mean and median of 7.2 kg s<sup>-1</sup> and 7.1 kg s<sup>-1</sup> respectively (Bani et al., 2012). In October 2007, a mean SO<sub>2</sub> flux of 8.0 ± 3.8 kg s<sup>-1</sup> across four days of traverses was reported by Métrich et al. (2011). A satellite-derived SO<sub>2</sub> flux of 6.8 to 23.3 kg s<sup>-1</sup> was estimated between 2000-2015, with a mean and median of 16.3 kg s<sup>-1</sup> and 19.2 kg s<sup>-1</sup> respectively (Carn et al., 2017). Comparisons in gas flux between different periods of observations and between methods must be treated with caution; they may, in discrete campaigns such as presented in this study, not represent broader changes through time.

### 3. UV Camera methods

Low-cost Raspberry Pi ultraviolet (UV) camera systems (the 'PiCams') were used to measure volcanic SO<sub>2</sub> outgassing, (Wilkes et al., 2017, 2016); in this case the units were modified to include 'PiJuice' hardware and software (<https://github.com/PiSupply/PiJuice>) to provide power to the Raspberry Pi boards which are at the heart of the camera system. The PiJuice units provide continuous supplies of power via lithium-polymer mobile phone batteries, which can be recharged using solar panels. In the field, both 1600 mAh and 2300 mAh batteries were used. With continuous solar charging (implementing 40 W solar panels for each Pi board) this configuration readily enabled field data acquisition for at least 6-7 hours per day in this location. This camera setup also involved omitting the GPS module included in the prior generation of the PiCam system, which automatically provided time synchronisation for the Raspberry Pi computers on start-up. Instead, in this configuration, GPS time synchronisation

was performed manually via the command line, expedited by the PiJuices' on board real-time-clock. The PiCam camera systems were furthermore equipped with two Edmund Optics Inc. filters (of full width at half maximum - 10 nm), centred around 310 and 330 nm, respectively, one for each lens, corresponding to spectral regions where SO<sub>2</sub> does and does not absorb incident UV radiation. As detailed further elsewhere, UV imaging systems in volcanic gas monitoring are predicated upon contrasting image intensities in these two wavebands, to isolate absorption in the image cause by sulphur dioxide absorption; for further details please see: (Gliß et al., 2017; Kantzas et al., 2010; Kern et al., 2015; McGonigle et al., 2017; Mori and Burton, 2006; Platt et al., 2015).

Two separate camera systems (Camera 1 and Camera 2) were set up viewing the plume simultaneously (enabling assessment of error and multiple plume angles simultaneously), from a position southwest of the summit crater from the treehouse site (~1900 m from the plume) at the Jungle Oasis, on 6<sup>th</sup> and 7<sup>th</sup> July, and from the Ash Plain Site (~2300 m from the plume) to the north-northwest on 8<sup>th</sup> and 9<sup>th</sup> July (see Figure 2 for locations). The UV cameras were also operated on the 11<sup>th</sup> July, however, in this case inclement weather and grounding of the plume prevented reliable data processing. During the measurement days, the plume direction varied from west to northwest, with dry and predominantly cloud-free weather (bar a brief period of rain on the 9<sup>th</sup> of July). Of the five days on which measurements were attempted, we acquired high quality data on four of the days, amassing 16 hours of high quality imagery overall across these days.

The camera images were captured with acquisition rates ranging 0.5 – 0.25 Hz, with additional collection of clear sky images prior to the plume sequences' capture, which are required in the processing routine to account for vignetting effects. Dark images were acquired per sequence too, to enable subtraction out of dark noise. We furthermore conducted frequent calibrations using gas cells with known SO<sub>2</sub> column densities (0 ppm m, 412 ppm m, and 1613 ppm m; with a manufacturer quoted error of 10%) between measurement sequences, not more than every 1-1.5 hours, with more frequent calibration when light conditions changed more rapidly. The data were then processed following the commonly applied protocols, already extensively referenced in the literature (D'Aleo et al., 2016; Kantzas et al., 2010; Kern et al., 2014; McGonigle et al., 2017), e.g., involving aligning images; selecting a clear sky background region; and choosing a plume cross-section along which to determine integrated column amounts (ICA), before multiplying by plume velocity to calculate flux. For the resulting flux data time series, we determined data distribution statistically with the Kolmogorov-Smirnov normality test to inform on appropriate measure of central tendency. The data were all non-normally distributed, therefore the median was used in the further calculations, detailed below. However, we continue to detail both mean and median values.

A goal of this study was to attempt to differentiate degassing fluxes from each of the vents. However, it was not possible to do this rigorously and at all times, given that changes in wind shear and crater-derived eddying led to time varying separation/overlap of these individual plumes (Pering et al., 2019b; Tamburello et al., 2013), creating difficulties in resolving emissions from the individual vents. Indeed, the plume predominantly appeared well-mixed on

emergence from the summit crater (Figure 2c). However, at times, the view from the Ash Plain site did allow us to identify gas pulses from the individual sources, likely associated with explosions, where distinct gas clouds from individual craters could be clearly spatially resolved (Figure 2d).

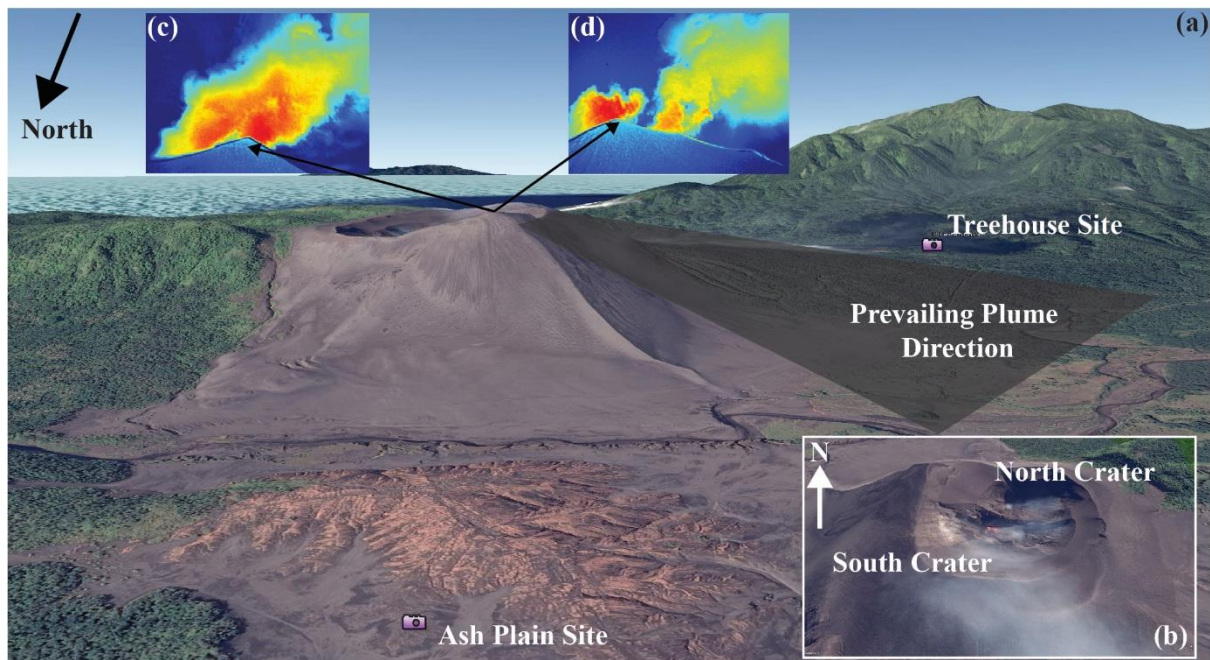


**Figure 2:** (a) An elevation-based perspective of the low summit of Yasur volcano, along with measurement positions and prevailing plume transport direction with inset (b) showing a close-up of the summit crater. In (c) there is a typical view of the plume with red colours representing higher concentrations of SO<sub>2</sub> showing clear mixing between plumes from different vents, and (d) shows an example of where it was possible to differentiate between emissions from both craters. Imagery is from Google Earth®.

### 3.1. Particle Image Velocimetry (PIV) for plume velocity determination.

One of the most significant, and yet frequently overlooked errors in UV camera image analysis is associated with plume velocity determination, for which three main methods are commonly used: cross-correlation (McGonigle et al., 2005; Williams-Jones et al., 2006), optical-flow (Delle Donne et al., 2019, 2017; Gliß et al., 2017; Kern et al., 2015; Peters et al., 2015; Peters and Oppenheimer, 2018), and manual tracking (Ilanko et al., 2019). The optimal method will largely be determined by the manifested plume conditions, as no single method is ideally suited to all situations. Manual tracking is suitable for stable plumes travelling at slow velocities, or for measurements at greater distances from the plume, where cross-correlation and optical-flow are less desirable, as the plume is more dilute and fewer pixels containing SO<sub>2</sub> are available for the analysis. Cross-correlation is preferred for broadly homogenous plumes that are well-mixed and undergo little turbulence (e.g., whereby eddying can cause SO<sub>2</sub> within parts of the plume to travel backwards relative to the bulk plume vector of motion e.g., the wind direction). Optical-flow methods are well suited to high velocity plumes, where the velocity field over the

plume profile is non-constant, e.g., due to pulsed gas outputs from craters, associated with strombolian explosions or puffing (Delle Donne et al., 2019, 2017; Liu et al., 2019; Peters et al., 2015).

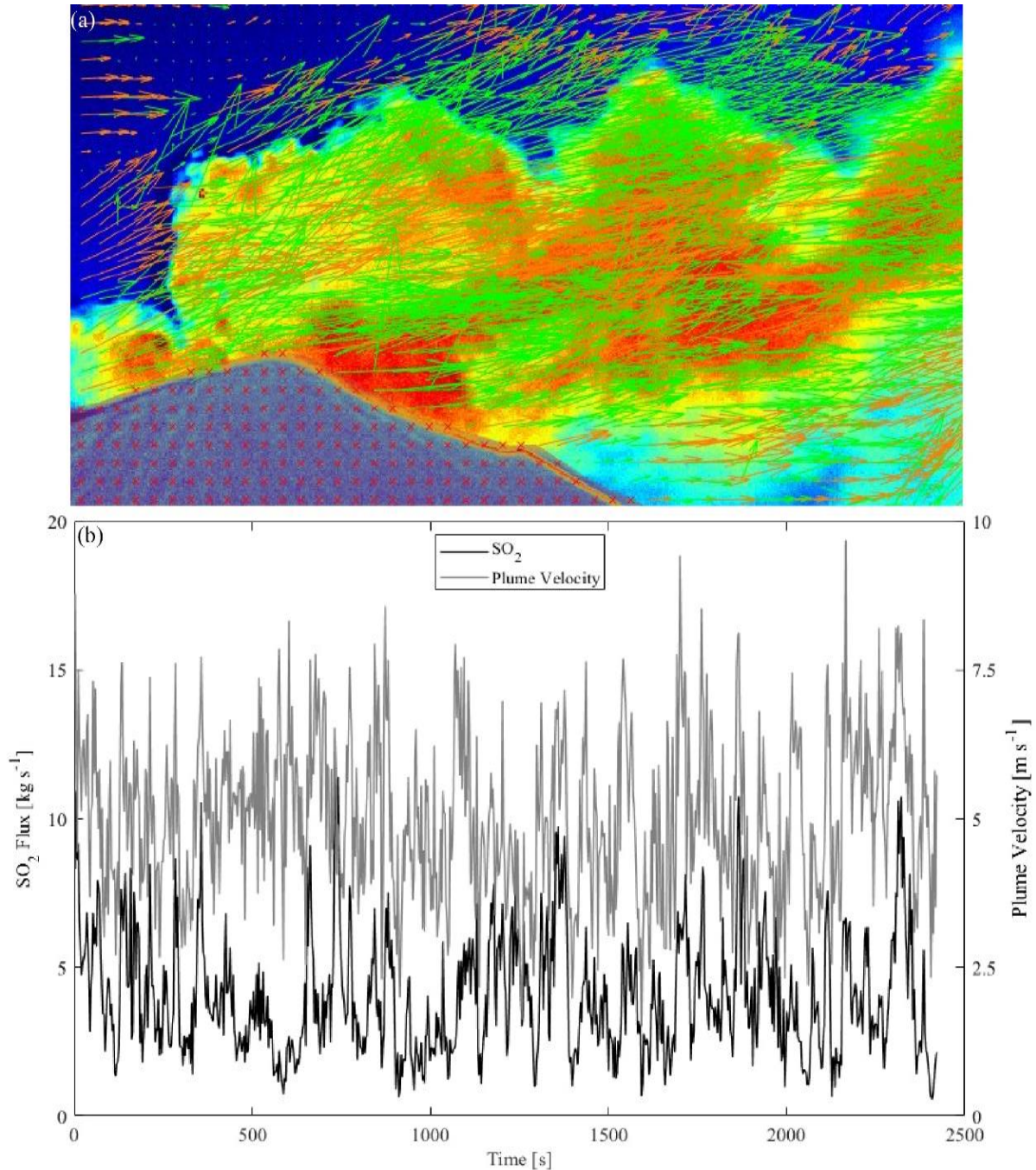


**Figure 3:** (a) example plume vectors generated during PIV analysis for one frame to another, superimposed over an SO<sub>2</sub> absorption image; and (b) example plume velocity and SO<sub>2</sub> fluxes for a time interval of 2500 seconds on the 7<sup>th</sup> July 2018, showing clear accelerations in plume velocities are evident during strombolian explosions.

In this study, we encountered difficulties in using these traditional methods. In particular, efficient mechanisms for tracking pulses of gas in a large dataset were required. Indeed, cross-



correlation sometimes failed, likely as a result of turbulent motion in the plume, and furthermore this approach does not cope well with transient increases in gas velocity, associated with impulsive gas release during strombolian explosions; hence this method is probably the least favourable in this context. A lack of structure in the plume appeared to lead to the failure of the Farneback optical flow algorithm (Gliß et al., 2017; Peters et al., 2015; Wilkes et al., 2017). We therefore instead adopted the use of Particle Image Velocimetry (PIV) for plume velocity determination, as briefly discussed in Kern et al., (2014). Previous use of PIV in a volcanic context has included tracking of lava lake velocity at Masaya (Pering et al. 2019) and similar to the pyroclast tracking velocimetry of (Gaudin et al., 2014a, 2014b). Here, we used PIVlab, a user-friendly MATLAB toolbox and app (Thielicke, 2014; Thielicke and Stamhuis, 2014). PIV works by comparing image pairs in sequences and looking for differences between them through two methods: direct cross-correlation and through the correlation of Fourier transforms. Both of these methods are conducted on integration areas (here we used three), with decreasing size on each pass. The end result is a velocity grid for the whole plume image, similar to those produced during the application of optical flow (Gliß et al., 2017; Peters et al., 2015), see Figure 3a.

We found that using PIV we were able to detect velocity differences in even the more homogenous plumes (i.e., with a quasi-uniform SO<sub>2</sub> distribution across most of the plume, except during strombolian explosions). PIV was used to extract velocity components corresponding to each image pixel, along, and perpendicular to, the integration line used in the ICA determination. In this case, rather than using a single plume velocity vector, perpendicular to the integration line, therefore, the plume velocity vectors per pixel were multiplied by the pixel's SO<sub>2</sub> column amount, and these sums were then integrated over the plume profile (see Figure 3). The PIV analyses show temporal and spatial variability in plume velocity, therefore, capturing a heterogeneity which is a real feature of the plume motion, yet not captured by cross-correlation or manual tracking. We report error for PIV analysis as the distance along the integration line at the plume range, corresponding to each pixel, divided by the lowest image capture frequency; for the Ash Plain Site this equates to an error of  $2 \pm 0.3 \text{ ms}^{-1}$  or  $\sim \pm 15\%$ , and for the Treehouse Site an error of  $5 \pm 0.6 \text{ ms}^{-1}$  or  $\sim 9\pm\%$ . These error estimates are based on typical plume velocities for each site.

### ***3.2. Estimation of a total UV Camera Measurement Error***

Here, we highlight the range of possible error sources, and perform additional analyses on our data pertaining specifically to: calibration curve drift, plume orientation, and plume distance. The final determined values for error are our best possible estimates on the basis of the available information and protocols applied in-the-field, which, wherever possible, were designed to minimise error.

The effects of light dilution have been quantified at a range of volcanic gas plume targets: SO<sub>2</sub> mass column amounts may be underestimated by  $\sim 10\text{-}60\%$  over a range of distances (2.1 km to 6.5 km) and conditions from hazy through to very clear (Campion et al., 2015). Light dilution has a larger effect during hazier conditions, which were not present during our successful

measurement days. Ilanko et al., (2019), calculated that at ~10.3 km distance from the plume (during clear conditions at Sabancaya volcano, Peru) SO<sub>2</sub> fluxes could be underestimated by 2.5 times, and at 4.25 km by 1.5 times (which would correspond to ~1.18 times [18%] at our maximum distance of 2300 m at Yasur). It is important to note that light dilution estimates are specific to each measurement location and given our range of distances to the plume and clear measurement conditions we suggest therefore that error relating to light dilution is <+20%. We also note that the plume was not optically thick, except following ash-rich strombolian explosions. Unfortunately, exact errors due to scattering of UV by ash are currently not quantifiable, but ash within the plume will likely lead to an underestimation of SO<sub>2</sub> column amounts (Kern et al., 2013; Tamburello et al., 2012). We attempted to minimise this error by integrating away from the summit area, where the plume is visibly less ash rich, and more transparent. We also further note that the peaks in gas flux from strombolian explosions are well defined within the resulting dataset (Figure 3).

**Table 1:** A summary of errors on UV camera measurements of SO<sub>2</sub> fluxes at Yasur Volcano in July 2018, including short comments and total RMS error.

	<b>Treehouse</b>	<b>Ash Plain</b>	<b>Comments</b>
<b>Distance</b>	1900 m	2300 m	-
<b>Description</b>	<b>Error</b>	<b>Error</b>	-
Light Dilution	+20%	+20%	Underestimation only, low given plume proximity.
Gas Cell Concentration	±10%	±10%	Manufacturer quoted
Calibration drift	±15%	±15%	Changing calibration conditions (see text)
Plume Velocity	±9	±15%	Based on pixel size (see text)
Plume Direction	±5%	±5%	Based on coincident UV camera data
Plume Distance	±18%	±18%	Based on plume deviation of 200 m.
Ash content	-	-	Underestimation, not quantifiable
<b>RMS Error</b>	-11.2% / +13.9%	-12.2% / +14.7%	Note the higher error related to underestimation (positive error).

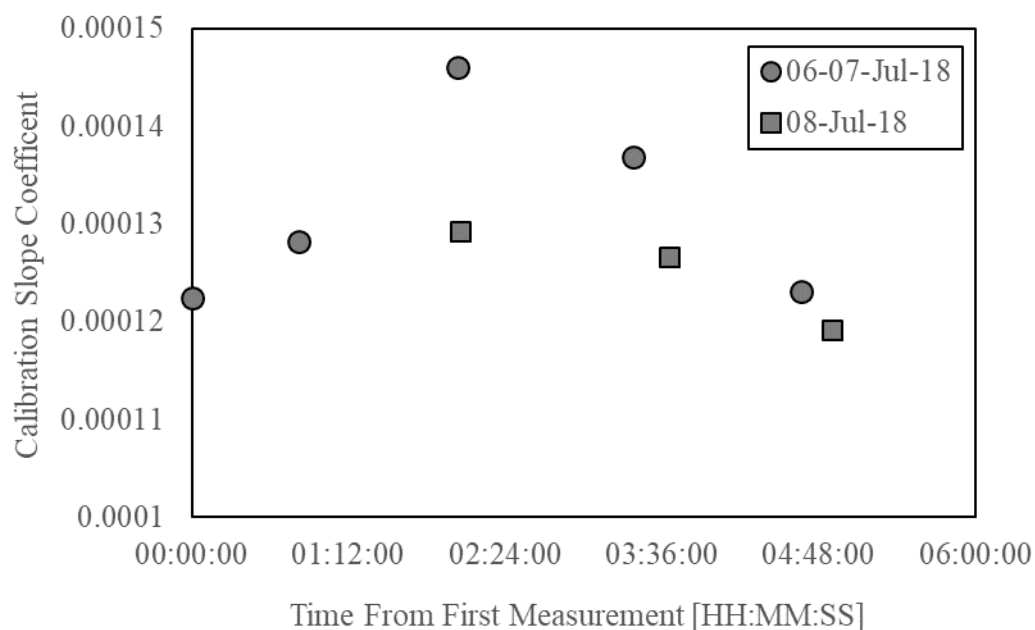


**Figure 4:** Example calibration slope coefficients (derived from regressions of gas cell concentrations against apparent absorbance) from two days of data. Timings are from the time of the first calibration on each of these measurement days. Note that the data peaks towards solar noon.

Gas cell calibration will alter throughout the day based on position of the sun and changing illumination as a result of background clouds, with changes in gas-cell calibrations potentially leading to over-estimation in  $\text{SO}_2$  column densities of up to 60% (Lübcke et al., 2013). Figure 4 shows the change in calibration slope coefficient (between regressions apparent absorbance coefficient and column density) throughout the day from time of first calibration (rather than using UTC), showing a variation from  $1.22 \times 10^{-4}$  to  $1.46 \times 10^{-4}$  in this parameter. When taking into account this characterised range in slope of  $2.4 \times 10^{-5}$ , and the broad assumption (for indicative illustration purposes) that there is a linear change between the first point and the highest point (corresponding to maximum solar zenith angle) we arrive, over the 122 minutes between these points, at a value of  $1.97 \times 10^{-7}$  increase in slope coefficient per minute. This would equate to a potential change in error of  $\sim 0.16\%$  per minute, which expanded over an hour could become 9.6% - or, for our maximum inter-calibration interval of  $\sim 95$  minutes, an error of 15.2%. It is possible therefore that any underlying trends in apparent gas emission rates below these thresholds are not differentiable from this error, i.e., an increase or decrease in flux at a rate of  $< \sim 0.16\%$  per minute. We suggest therefore that errors from cell calibration (notwithstanding the  $\sim \pm 10\%$  manufacturer quoted cell content error) amount to a maximum of  $\sim \pm 15\%$  for our measurement period.

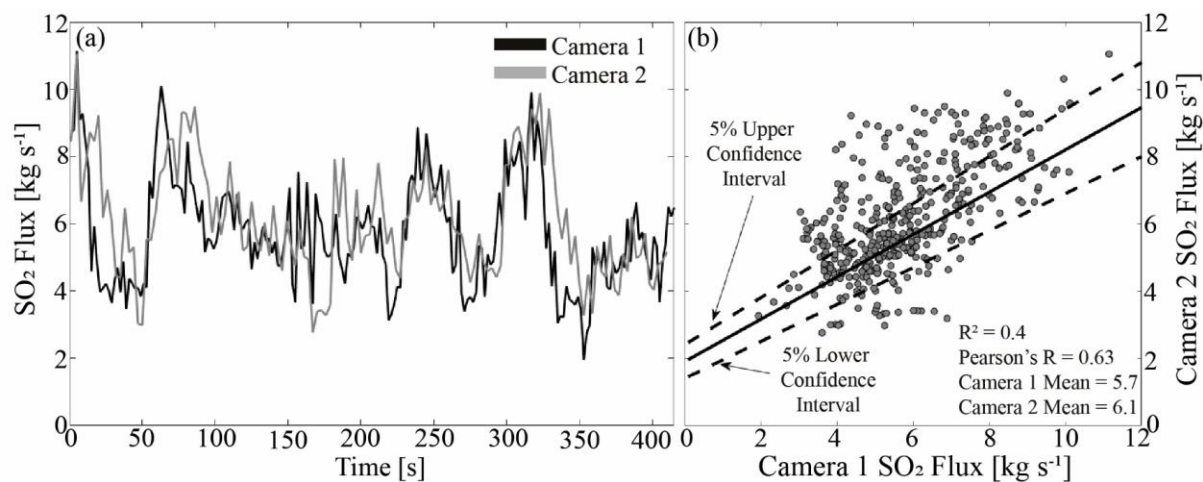


**Figure 5:** (a) Example period of overlapping data from two separately acquiring synchronous cameras, viewing the plume from slightly different orientations. One dataset has been shifted by the lag value which generated the maximum correlation coefficient, following cross-correlation between the two series, in an attempt to best temporally match the data. Note that there are differences in the magnitudes of peaks and troughs in the different datasets, even when shifted relative to one another in this way, due to smoothing or turbulence during plume movement through the atmosphere and the slightly different views of the units through the plume. In (b) a linear regression model ( $R^2 = 0.4$ ) is shown, demonstrating the best fit between time series data from the two cameras, as well as confidence intervals. The statistical parameters are similar, but there are differences in peaks and troughs between the two datasets.

We used fixed distances of 1900 m and 2300 m from the camera to the plume for our retrieval calculations in the cases of data from the treehouse and Ash Plain sites, respectively. For the Ash Plain data, we determined, therefore that a 100 m error in plume distance leads to a < 5% difference in computed gas masses across the plume cross section (with underestimation in this distance corresponding to underestimation in gas mass), and a 200 m error in distance to < 9% error. Comparisons of the same test dataset with different velocities in PIV analyses showed variations from 1 – 7 % with the 100 m distance and 5 – 11% in the 200 m case. The combined effect of these distance uncertainties on mass and velocity gives a 7-10% error in fluxes for 100 m distance to plume error, and 16-18 % for 200 m. We therefore take the maximum value here of ~18% and apply this conservatively, to our entire dataset.

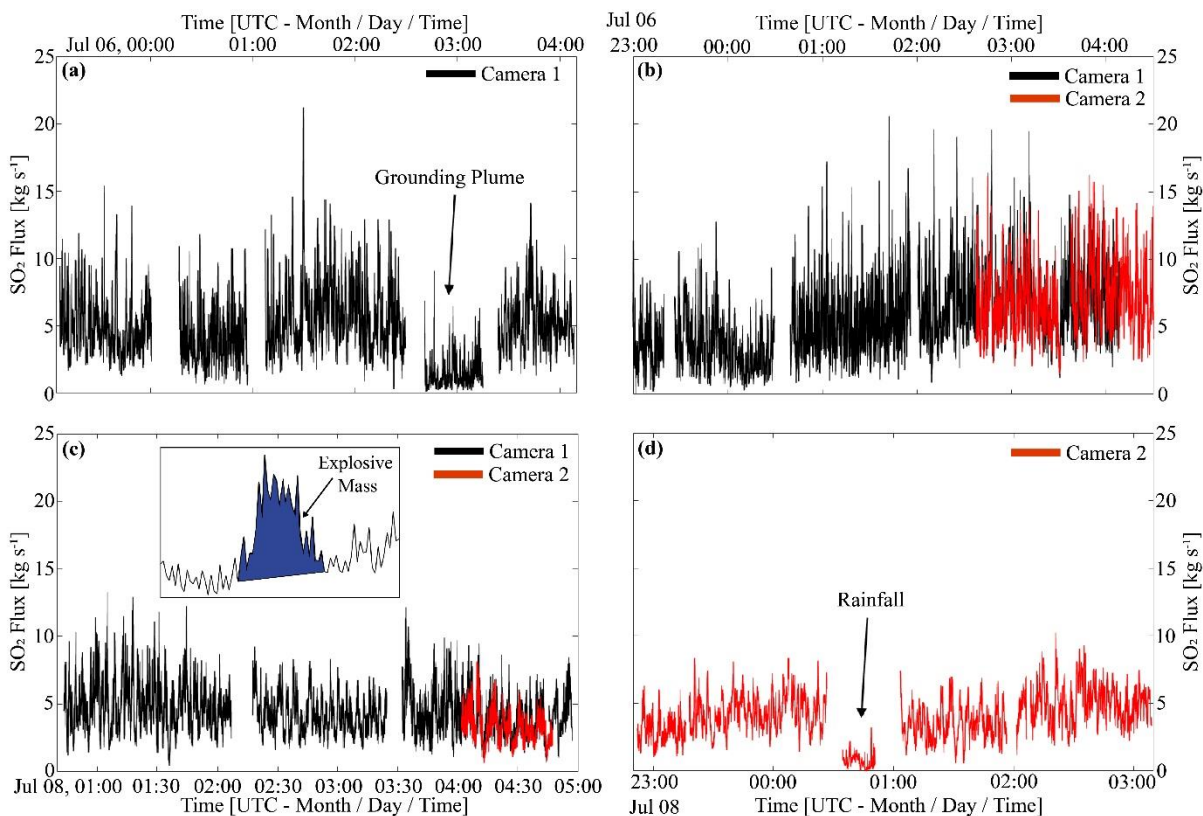


**Figure 6:** (a) through (d) show retrieved gas fluxes, where clear peaks correspond to strombolian explosions, for all the image data captured during the observation period; also highlighted are periods where the plume was grounded in (a) and heavy rainfall was encountered in (d). Inset in (c) is an example of explosive mass determination, where integration occurs below the explosion peak (e.g., shaded blue area), above background levels.

Given changes in plume direction, the orientation with which the integration line bisects the plume is also relevant in consideration of measurement uncertainty (Klein et al., 2017). To investigate this, we use overlaps between data from two synchronously-acquiring cameras (Figure 5), which had slightly different plume views and hence integration line orientations relative to the plume geometry, simulating the time dependent effect of the plume vector moving, in response to changing wind conditions, with respect to a fixed integrated column amount line. In this case the two datasets were cross-correlated and shifted by the lag corresponding to the maximum correlation to account for different transport times from the source to the two cameras' different integration lines. The calculated difference in flux retrieval from the two units, based on comparing the acquired median values per unit is  $\sim\pm 5\%$ .

In addition, we also report computed flux data in Figure 6 (which documents the retrieved data from the entire campaign) during periods when the plume grounded, e.g., the integration line could not cover the entire plume cross section, as well as episodes of heavy rainfall. During these periods, median SO<sub>2</sub> fluxes were underestimated significantly by  $\sim 4.3$ - $4.4$  and  $5.6$ - $7.3$  times, respectively, based on comparison with median values of retrieved fluxes either side of these episodes. Whilst the data captured under these circumstances were not used in the

foregoing analysis, nor considered representative of the volcanic outgassing, they are reported here, to illustrate the significant error these effects give rise to.

**Table 2.** A summary of measurement durations and SO<sub>2</sub> flux statistics for daily UV camera measurements at Yasur Volcano in July 2018.

<b>Date (UTC)</b>	<b>05-06/07/18</b>	<b>06-07/07/18</b>	<b>08/07/18</b>	<b>08-09/07/18</b>
<b>Date (Local)</b>	<b>06/07/18</b>	<b>07/07/18</b>	<b>08/08/18</b>	<b>09/08/18</b>
Time series duration (hh:mm)	4:15	04:42	03:54	03:33
Total time (hh:mm)	05:01	05:31	04:14	04:17
Mean (kg/s)	5.2	5.5	4.5	4.1
Median (kg/s)	4.7	5.1	4.2	4.0

## 4. Results and Discussion

### 4.1 SO<sub>2</sub> Fluxes and estimates of the Masses of gas emitted during strombolian explosions

Time series gas fluxes are shown in Figure 6, with a summary of daily statistics in Table 1. The median flux across the four days of measurements was 4.5 kg s<sup>-1</sup> and the mean was 4.9 kg s<sup>-1</sup>, reflecting the peaks in SO<sub>2</sub> flux associated with frequent strombolian explosions. These gas fluxes correspond to a daily median and mean of 389 and 423 t d<sup>-1</sup> across the measurement period. Daily statistics are given in Table 2: median SO<sub>2</sub> fluxes ranged between 4.0 to 5.1 kg s<sup>-1</sup> across the measurement days and the daily means were 4.1 to 5.5 kg s<sup>-1</sup>. The timeseries data are suggestive of gradual changes in background SO<sub>2</sub> emissions over several hours, but it is not clear whether these are real or a product of artefact error. A shift in activity is, however, plausible based on the observation of large strombolian explosions with visible ballistics and shockwaves, particularly on 8<sup>th</sup> and 9<sup>th</sup> July, when lower fluxes were measured.

Masses of SO<sub>2</sub> released during each strombolian explosion were calculated by integrating beneath the explosive pulse and summing the total SO<sub>2</sub> released, after Tamburello *et al.*, (2012), see Figure 6c. Although, a challenge here is that strombolian explosions were not visible within the imagery (i.e., vents were at depth within the crater). We use two methods to determine when explosions occurred within the UV camera imagery: firstly, when gas pulses in the camera images are observed to originate and visibly accelerate above the rim of the summit crater (see Figure 1a); secondly, where gas burst traces are manifested in the flux time series, showing the characteristic coda (a period of elevated flux following a strombolian explosions which gradually declines) detailed in Pering *et al.*, (2016), see Figure 6c. The number of explosions is probably underestimated using these methods; however, the resulting estimation of SO<sub>2</sub> released during each explosion is useful for comparison to literature values (Table 3). Overall, SO<sub>2</sub> masses released were estimated for 135 explosions, across five days. Mean masses of SO<sub>2</sub> released increased from 6<sup>th</sup> to 9<sup>th</sup> July 2018, which is consistent with visual observations of more powerful explosions on 8 and 9 July 2018.

**Table 3:** A breakdown of daily SO<sub>2</sub> explosion mass data. Also displayed are ratio data in percentage terms, concerning the portioning of gas fluxes between passive and explosive release. Lower and Upper ratios refer to the ranges indicated in determined active molar ratios by (Woitischek et al., 2020; Table 3 - CO<sub>2</sub>/SO<sub>2</sub> = 2.85 ± 0.17; H<sub>2</sub>O/SO<sub>2</sub> = 315 ± 71.8; SO<sub>2</sub>/HCl = 1.6 ± 0.22).

Date (UTC)	05/07/2018	06/07/2018	07/07/2018	08/07/2018	09/07/2019	Total
Explosions Counted	8	43	39	36	9	<b>135</b>
						<b>Mean</b>
SO <sub>2</sub> Min (kg)	10.2	8.9	8	12	10	<b>9.8</b>
SO <sub>2</sub> Mean (kg)	26.9	22.1	27	39	45	<b>32.0</b>
SO <sub>2</sub> Max (kg)	64.1	44.9	62	81	69	<b>64.2</b>
Passive %	66	64	70	78	68	<b>69</b>
Explosive %	34	36	30	22	32	<b>31</b>
<b>Lower Ratios</b>						
Total – Min (kg)	712	625	575	822	721	<b>691</b>
Total – Mean (kg)	1884	1550	1892	2713	3164	<b>2241</b>
Total – Max (kg)	3020	3148	4370	5678	4813	<b>4206</b>
<b>Middle Ratios</b>						
Total – Min (kg)	940	824	759	1084	952	<b>912</b>
Total – Mean (kg)	2486	2046	2497	3579	4175	<b>2957</b>
Total – Max (kg)	5929	4153	5767	7493	6350	<b>5938</b>
<b>Upper Ratios</b>						
Total – Min (kg)	1167	1024	942	1347	1182	<b>1132</b>
Total – Mean (kg)	3088	2541	3102	4446	5186	<b>3673</b>
Total – Max (kg)	7365	5159	7163	9307	7888	<b>7376</b>

The range of SO<sub>2</sub> masses released during strombolian explosions at Yasur, of 8 – 69 kg (mean 32 kg) are similar to those estimated by Tamburello et al., (2012) at Stromboli, who found a range of 2 – 55 kg (mean of 20 kg); but higher than those observed at Etna during mild strombolian activity (Pering et al., 2015), which ranged from 0.1 to 14 kg. Gas ratios (SO<sub>2</sub>, H<sub>2</sub>S, H<sub>2</sub>O and CO<sub>2</sub>) derived from a combined Fourier transform infrared spectroscopy (FTIR) and Multi-GAS study from 6<sup>th</sup> to 16<sup>th</sup> July 2018 show distinct gas compositions during passive and explosive activity (Woitischek et al., 2020). Gas emitted during active (strombolian) activity had molar ratios of: CO<sub>2</sub>/SO<sub>2</sub> = 2.85 ± 0.17; H<sub>2</sub>O/SO<sub>2</sub> = 315 ± 71.8; SO<sub>2</sub>/HCl = 1.7 ± 0.22. Using these data we can estimate total gas slug masses, shown in Table 3. The mean total gas mass emitted during strombolian explosions at Yasur is ~2960 kg, with a range of 910 – 5940 kg. These estimates are similar to the range of 170 – 1674 kg for strombolian explosions at Pacaya (Dalton et al., 2010); whilst at Stromboli values range 44 to 238 kg according to Barnie et al. (2015) and 2 to 1425 kg as determined by Delle Donne et al. (2016).

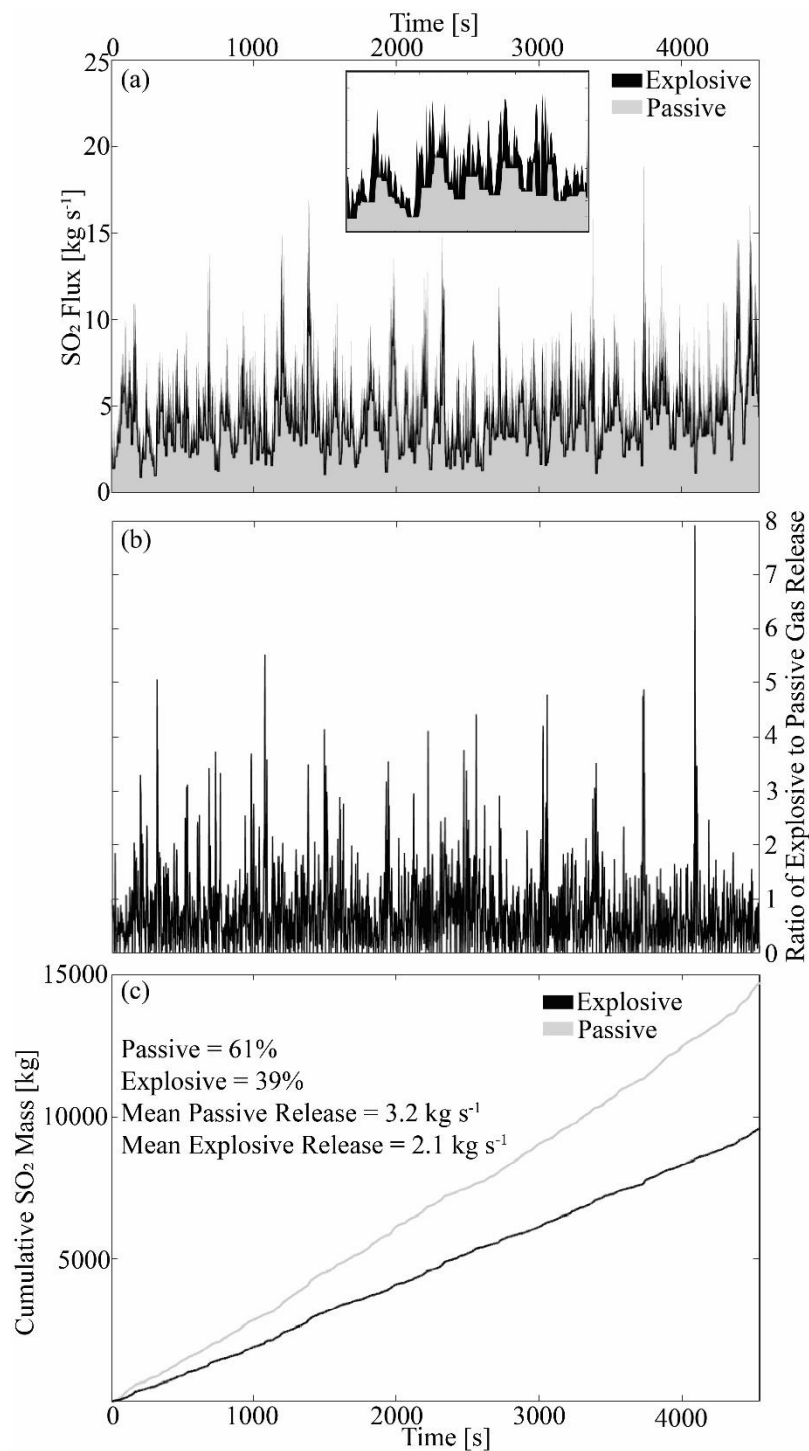


**Figure 7:** (a) Separation of passive and explosion gas release for a period on the 7<sup>th</sup> July with (inset) a zoomed illustration of the simple statistical moving minimum based model, showing oscillation in background passive degassing overtopped by explosive contributions; (b) the ratio of passive to explosive degassing; and (v) a cumulative plot showing the division between passive and explosive gas release, here passive and explosive release have been cumulatively summed to show the change through time at the sampling frequency. The passive to explosive ratio is then the ratio of the final sum of gas release.



## 4.2. Simple Statistical Separation of Passive and Explosive Degassing

Others have studied the ratios of explosive to passive release during strombolian explosions on Stromboli (Tamburello et al., 2012) and Etna (Pering et al., 2015). Here, we attempt to expand on this by using a simple statistical measure involving the moving minimum (which traces the lower values in dataset over a defined window, much as the moving mean), to estimate the passive release of gas through time, which, when subtracted from total flux, provides an approximate estimate of passive vs. explosive release. This was necessary as our manual selection of events likely missed a proportion of strombolian explosions and is similar to the automated method of Delle Donne et al., (2017), which involved finding local peaks. For an example period (Figure 7) we highlight the moving minimum, which is set to a window size of 20 s, which is generally the characteristic timeframe of large peaks and troughs associated with strombolian explosions (Delle Donne et al., 2017; Pering et al., 2016). Note that, using this moving minimum method, an oscillation (non-uniform) background is apparent. This is similar to that of Delle Donne et al., (2017), who showed fluctuation in passive background below strombolian explosions and is used as a best estimate to solely extract the explosive contribution. In this instance, at Yasur, a moving minimum over this window proved best, given the higher frequency of explosive events; however, with a greater timeframe between events, the moving median may be a better measure. We also prefer this statistical estimation technique over using our estimated SO<sub>2</sub> masses, given that the latter required manual selection of strombolian explosions. This simple moving minimum approach could be readily and simply automated for routine monitoring of activity from strombolian explosion producing volcanic systems.

Daily estimates of the passive and active degassing contributions are shown in Table 3, with a mean of 69% passive to 31% explosive. These estimates are similar to those estimated at Stromboli: 77% passive to 23% explosive (termed active which also includes puffing); and Etna: 67% passive to 33% explosive (Pering et al., 2015). These datasets serve to illustrate the dominance of passive degassing in the gas emission budget at volcanoes that exhibit strombolian activity. On the 8<sup>th</sup> July 2018 we calculated a higher passive degassing contribution, at 78%. This day was characterised by higher SO<sub>2</sub> masses emitted during individual explosions, but lower overall SO<sub>2</sub> fluxes. These features may be consistent with a degassing magma column beneath a thicker, more viscous and impermeable crystal-rich plug, requiring a higher gas mass to drive more powerful explosions (Polacci et al., 2012; Simons et al., 2020; Woitischek et al. 2020), which is consistent with visual observations.

## 4.3. Models of gas slug behaviour

Using our determined values for total slug mass, we can estimate slug lengths using the static pressure model of (Del Bello et al., 2012). We use fixed values of 2600 kg m<sup>3</sup> and 1000 Pa s<sup>-1</sup> for density and viscosity, respectively, with an atmospheric pressure of 101,325 Pa. The only parameter we vary in the model is that of conduit diameter, which we step from 3 m to 7 m. We use only the mean explosive gas ratios and masses (and not the range obtained when including error) for simplicity. It should be noted that the molar H<sub>2</sub>O/SO<sub>2</sub> ratio is high and

variable (Woitischek et al., 2020). As water is the gas contributing most to the mass of the slug, it is likely that our determined total gas masses are an overestimation. Our results are summarised in Table 4. We determine slug lengths ranging 188 – 609 m (median and mean of 347 m and 366 m respectively) for a conduit diameter of 3 m, however, this reduces to 76 – 260 m (median and mean of 146 and 154 m respectively) for a conduit diameter of 7 m. Kremers et al. (2013) calculated lower values of 59 – 244 m using seismo-acoustic data, and it would therefore seem that a larger conduit diameter may be more plausible at Yasur, which may bifurcate or split at very shallow depths (Simons et al., 2020).

**Table 4:** A summary of gas slug volumes and lengths using the model of Del Bello et al. (2012) and based on gas flux and composition data acquired during strombolian activity at Yasur Volcano in July 2018.

<b>Statistic</b>	<b>Slug Volume (m<sup>3</sup>)</b>	<b>D = 3 m</b>	<b>D = 4 m</b>	<b>D = 5 m</b>	<b>D = 6 m</b>	<b>D = 7 m</b>
Min	4286	188	139	110	90	76
Median	14055	347	259	205	170	146
Mean	15556	366	272	217	180	154
Max	42337	609	455	364	303	260

## 5. Summary and Conclusions

In this work we highlighted the utility of using low-cost solar-powered Raspberry Pi UV cameras for prolonged field campaigns. We continuously imaged the volcanic plume to yield both velocity, using a PIV method (Thielicke, 2014; Thielicke and Stamhuis, 2014), and SO<sub>2</sub> fluxes over periods of several hours per day, at temporal resolutions of up to 0.5 Hz with brief pauses for calibration. SO<sub>2</sub> fluxes were determined, with daily means of 4.1-5.5 kg s<sup>-1</sup> (medians from 4.0-5.1 kg s<sup>-1</sup>) which are within the ranges of those measured previously at Yasur using ground-based methods of 2.5 to 17.2 kg s<sup>-1</sup> (Bani et al., 2012; Bani and Lardy, 2007). SO<sub>2</sub> masses emitted during individual strombolian explosions ranged from 8-81 kg, similar to events at Stromboli, which were associated with the emission of 2 – 55 kg SO<sub>2</sub> (Tamburello et al., 2012). By using a simple statistical measure we estimate that passive degassing, at 69%, is the dominant mode of degassing at Yasur, compared to 31% explosive. Observations suggest that periods of lower gas output are associated with conduit sealing and more violent explosions, however, a longer dataset would be needed to test this hypothesis substantively. By combining SO<sub>2</sub> explosion masses with gas ratios (Woitischek et al., 2020) we determined total explosion gas masses of mean ~910-5940 kg, which correspond to slug lengths, using the model of Del Bello et al. (2012) of ~76-260 m, if a larger conduit diameter of ~7 m is used. Smaller conduit diameters lead to longer slug lengths ~188-600 m at 3 m diameter, larger than those estimated previously of ~59 – 244 m (Kremers et al., 2013). The data presented here represent an important addition to our gas data based characterisation of the spectrum of strombolian activity across the globe.

## 6. Acknowledgements

We would like to thank the Vanuatu Meteorology and Geo-hazards Department for permission to conduct this fieldwork, Kelson and Joyce Hosea for their hospitality at the Jungle Oasis, and Roger for his assistance in the field. J.W and M.E. were supported by the Natural Environment Research Council (grant number NE/L002507/1), by the postgraduate travel funds received from Fitzwilliam College, by the Elspeth Matthews grant given by the Royal Geological Society, by the Mary Euphrasia Mosley, Sir Bartle Frere and Worts travel fund report given by the University of Cambridge and by the Exzellenzstipendium received by WKO. A.A. acknowledges funding support from the Alfred P. Sloan Foundation via the Deep Carbon Observatory (UniPa-CiW subcontract 10881-1262) and from MIUR (under grant n. PRIN2017-2017LMNLAW). T.D.P. acknowledges the support of the Royal Society (RG170226). T.I. is a Commonwealth Rutherford Fellow, funded by the UK government. A.McG. acknowledges support from the Rolex Institute.

## 7. References

- Aiuppa, A., Coco, E. Lo, Liuzzo, M., Giudice, G., 2016. Terminal Strombolian activity at Etna's central craters during summer 2012: The most CO<sub>2</sub>-rich volcanic gas ever recorded at Mount Etna. *Geochemical*.
- Aiuppa, A., Federico, C., Giudice, G., Gurrieri, S., 2005. Chemical mapping of a fumarolic field: La Fossa Crater, Vulcano Island (Aeolian Islands, Italy). *Geophys. Res. Lett.* 32, L13309. <https://doi.org/10.1029/2005GL023207>
- Bani, P., Lardy, M., 2007. Sulphur dioxide emission rates from Yasur volcano, Vanuatu archipelago. *Geophys. Res. Lett.* 34. <https://doi.org/10.1029/2007GL030411>
- Bani, P., Oppenheimer, C., Allard, P., Shinohara, H., Tsanev, V., Carn, S., Lardy, M., Garaebiti, E., 2012. First estimate of volcanic SO<sub>2</sub> budget for Vanuatu island arc. *J. Volcanol. Geotherm. Res.* 211–212, 36–46. <https://doi.org/10.1016/j.jvolgeores.2011.10.005>
- Barnie, T., Bombrun, M., Burton, M.R., Harris, A., Sawyer, G., 2015. Quantification of gas and solid emissions during Strombolian explosions using simultaneous sulphur dioxide and infrared camera observations. *J. Volcanol. Geotherm. Res.* 300, 167–174. <https://doi.org/10.1016/j.jvolgeores.2014.10.003>
- Barth, A., Edmonds, M., Woods, A., 2019. Valve-like dynamics of gas flow through a packed crystal mush and cyclic strombolian explosions. *Sci. Rep.* 9, 821. <https://doi.org/10.1038/s41598-018-37013-8>
- Battaglia, A., Bitetto, M., Aiuppa, A., Rizzo, A.L., Chigna, G., Watson, I.M., D'Aleo, R., Juárez Cacao, F.J., de Moor, M.J., 2018. The Magmatic Gas Signature of Pacaya Volcano, With Implications for the Volcanic CO<sub>2</sub> Flux From Guatemala. *Geochemistry, Geophys. Geosystems* 19, 667–692. <https://doi.org/10.1002/2017GC007238>
- Blackburn, E.A., Wilson, L., Sparks, R.S.J., 1976. Mechanisms and dynamics of strombolian activity. *J. Geol. Soc. London.* 132, 429–440. <https://doi.org/10.1144/gsjgs.132.4.0429>
- Branca, S., Del Carlo, P., 2005. Types of eruptions of Etna volcano AD 1670-2003: Implications for short-term eruptive behaviour. *Bull. Volcanol.* 67, 732–742. <https://doi.org/10.1007/s00445-005-0412-z>
- Burton, M., Allard, P., Mure, F., La Spina, A., 2007. Magmatic Gas Composition Reveals the Source Depth of Slug-Driven Strombolian Explosive Activity. *Science* (80-. ). 317, 227–230. <https://doi.org/10.1126/science.1141900>
- Campion, R., Delgado-Granados, H., Mori, T., 2015. Image-based correction of the light

- dilution effect for SO<sub>2</sub> camera measurements. *J. Volcanol. Geotherm. Res.* 300, 48–57.  
<https://doi.org/10.1016/j.jvolgeores.2015.01.004>
- Carn, S.A., Fioletov, V.E., Mclinden, C.A., Li, C., Krotkov, N.A., 2017. A decade of global volcanic SO<sub>2</sub> emissions measured from space. *Sci. Rep.* 7, 1–12.  
<https://doi.org/10.1038/srep44095>
- Chouet, B., Dawson, P., Ohminato, T., Martini, M., Saccorotti, G., Giudicepietro, F., De Luca, G., Milana, G., Scarpa, R., 2003. Source mechanisms of explosions at Stromboli Volcano, Italy, determined from moment-tensor inversions of very-long-period data. *J. Geophys. Res. Solid Earth* 108, 2019. <https://doi.org/10.1029/2002JB001919>
- D'Aleo, R., Bitetto, M., Delle Donne, D., Tamburello, G., Battaglia, A., Coltelli, M., Patanè, D., Prestifilippo, M., Sciotto, M., Aiuppa, A., 2016. Spatially resolved SO<sub>2</sub> flux emissions from Mt Etna. *Geophys. Res. Lett.* 43, 7511–7519.  
<https://doi.org/10.1002/2016GL069938>
- Dalton, M.P., Waite, G.P., Watson, I.M., Nadeau, P.A., 2010. Multiparameter quantification of gas release during weak Strombolian eruptions at Pacaya Volcano, Guatemala. *Geophys. Res. Lett.* 37. <https://doi.org/10.1029/2010GL042617>
- Del Bello, E., Llewellyn, E.W., Taddeucci, J., Scarlato, P., Lane, S.J., 2012. An analytical model for gas overpressure in slug-driven explosions: Insights into Strombolian volcanic eruptions. *J. Geophys. Res. Solid Earth* 117. <https://doi.org/10.1029/2011JB008747>
- Delle Donne, D., Aiuppa, A., Bitetto, M., D'aleo, R., Coltelli, M., Coppola, D., Pecora, E., Ripepe, M., Tamburello, G., 2019. Changes in SO<sub>2</sub> Flux Regime at Mt. Etna Captured by Automatically Processed Ultraviolet Camera Data. *Remote Sens.* 11, 1201.  
<https://doi.org/10.3390/rs11101201>
- Delle Donne, D., Ripepe, M., 2012. High-frame rate thermal imagery of strombolian explosions: Implications for explosive and infrasonic source dynamics. *J. Geophys. Res. Solid Earth* 117, 1–12. <https://doi.org/10.1029/2011JB008987>
- Delle Donne, D., Ripepe, M., Lacanna, G., Tamburello, G., Bitetto, M., Aiuppa, A., 2016. Gas mass derived by infrasound and UV cameras: Implications for mass flow rate. *J. Volcanol. Geotherm. Res.* 325, 169–178.  
<https://doi.org/10.1016/j.jvolgeores.2016.06.015>
- Delle Donne, D., Tamburello, G., Aiuppa, A., Bitetto, M., Lacanna, G., D'Aleo, R., Ripepe, M., 2017. Exploring the explosive-effusive transition using permanent ultraviolet cameras. *J. Geophys. Res. Solid Earth* 122, 4377–4394.  
<https://doi.org/10.1002/2017JB014027>
- Dibble, R.R., Kyle, P.R., Rowe, C.A., 2008. Video and seismic observations of Strombolian eruptions at Erebus volcano, Antarctica. *J. Volcanol. Geotherm. Res.* 177, 619–634.  
<https://doi.org/10.1016/j.jvolgeores.2008.07.020>
- Firth, C.W., Handley, H.K., Cronin, S.J., Turner, S.P., 2014. The eruptive history and chemical stratigraphy of a post-caldera, steady-state volcano: Yasur, Vanuatu. *Bull. Volcanol.* 76, 1–23. <https://doi.org/10.1007/s00445-014-0837-3>
- Garcés, M.A., Hagerty, M.T., Schwartz, S.Y., 1998. Magma acoustics and time-varying melt properties at Arenal Volcano, Costa Rica. *Geophys. Res. Lett.* 25, 2293–2296.  
<https://doi.org/10.1029/98GL01511>
- Gaudin, D., Moroni, M., Taddeucci, J., Scarlato, P., Shindler, L., 2014a. Pyroclast Tracking Velocimetry: A particle tracking velocimetry-based tool for the study of Strombolian explosive eruptions. *J. Geophys. Res. Solid Earth* 119, 5369–5383.  
<https://doi.org/10.1002/2014JB011095>
- Gaudin, D., Taddeucci, J., Scarlato, P., del Bello, E., Ricci, T., Orr, T., Houghton, B., Harris, A., Rao, S., Bucci, A., 2017a. Integrating puffing and explosions in a general scheme for Strombolian-style activity. *J. Geophys. Res. Solid Earth* 122, 1860–1875.

- <https://doi.org/10.1002/2016JB013707>
- Gaudin, D., Taddeucci, J., Scarlato, P., Harris, A., Bombrun, M., Del Bello, E., Ricci, T., 2017b. Characteristics of puffing activity revealed by ground-based, thermal infrared imaging: the example of Stromboli Volcano (Italy). *Bull. Volcanol.* 79, 24. <https://doi.org/10.1007/s00445-017-1108-x>
- Gaudin, D., Taddeucci, J., Scarlato, P., Moroni, M., Freda, C., Gaeta, M., Palladino, D.M., 2014b. Pyroclast Tracking Velocimetry illuminates bomb ejection and explosion dynamics at Stromboli (Italy) and Yasur (Vanuatu) volcanoes. *J. Geophys. Res. Solid Earth* 119, 5384–5397. <https://doi.org/10.1002/2014JB011096>
- Gliß, J., Stebel, K., Kylling, A., Dinger, A., Sihler, H., Sudbø, A., Gliß, J., Stebel, K., Kylling, A., Dinger, A.S., Sihler, H., Sudbø, A., 2017. Pyplis—A Python Software Toolbox for the Analysis of SO<sub>2</sub> Camera Images for Emission Rate Retrievals from Point Sources. *Geosciences* 7, 134. <https://doi.org/10.3390/geosciences7040134>
- Illanko, T., Oppenheimer, C., Burgisser, A., Kyle, P., 2015. Cyclic degassing of Erebus volcano, Antarctica. *Bull. Volcanol.* 77, 56. <https://doi.org/10.1007/s00445-015-0941-z>
- Illanko, T., Pering, T., Wilkes, T., Apaza Choquehuayta, F., Kern, C., Díaz Moreno, A., De Angelis, S., Layana, S., Rojas, F., Aguilera, F., Vasconez, F., McGonigle, A., 2019. Degassing at Sabancaya volcano measured by UV cameras and the NOVAC network. *Volcanica* 2, 239–252. <https://doi.org/10.30909/vol.02.02.239252>
- James, M.R., Lane, S.J., Corder, S.B., 2008. Modelling the rapid near-surface expansion of gas slugs in low-viscosity magmas. *Geol. Soc. London, Spec. Publ.* 307, 147–167. <https://doi.org/10.1144/GSL.SP.2003.213.01.17>
- James, M.R., Lane, S.J., Wilson, L., Corder, S.B., 2009. Degassing at low magma-viscosity volcanoes: Quantifying the transition between passive bubble-burst and Strombolian eruption. *J. Volcanol. Geotherm. Res.* 180, 81–88. <https://doi.org/10.1016/j.jvolgeores.2008.09.002>
- Jaupart, C., Vergnolle, S., 1989. The generation and collapse of a foam layer at the roof of a basaltic magma chamber. *J. Fluid Mech.* 203, 347–380. <https://doi.org/10.1017/S0022112089001497>
- Jaupart, C., Vergnolle, S., 1988. Laboratory models of Hawaiian and Strombolian eruptions. *Nature* 331, 58–60. <https://doi.org/10.1038/331058a0>
- Johnson, J.B., Aster, R.C., 2005. Relative partitioning of acoustic and seismic energy during Strombolian eruptions. *J. Volcanol. Geotherm. Res.* 148, 334–354. <https://doi.org/10.1016/j.jvolgeores.2005.05.002>
- Johnson, J.B., Ripepe, M., 2011. Volcano infrasound: A review. *J. Volcanol. Geotherm. Res.* 206, 61–69. <https://doi.org/10.1016/J.JVOLGEORES.2011.06.006>
- Kantzas, E.P., McGonigle, A.J.S., Tamburello, G., Aiuppa, A., Bryant, R.G., 2010. Protocols for UV camera volcanic SO<sub>2</sub> measurements. *J. Volcanol. Geotherm. Res.* 194, 55–60. <https://doi.org/10.1016/j.jvolgeores.2010.05.003>
- Kern, C., Lübcke, P., Bobrowski, N., Campion, R., Mori, T., Smekens, J.-F., Stebel, K., Tamburello, G., Burton, M., Platt, U., Prata, F., 2015. Intercomparison of SO<sub>2</sub> camera systems for imaging volcanic gas plumes. *J. Volcanol. Geotherm. Res.* 300, 22–36. <https://doi.org/10.1016/j.jvolgeores.2014.08.026>
- Kern, C., Sutton, J., Elias, T., Lee, L., Kamibayashi, K., Antolik, L., Werner, C., 2014. An automated SO<sub>2</sub> camera system for continuous, real-time monitoring of gas emissions from Kīlauea Volcano’s summit Overlook Crater. *J. Volcanol. Geotherm. Res.* 300, 81–94. <https://doi.org/10.1016/j.jvolgeores.2014.12.004>
- Kern, C., Werner, C., Elias, T., Sutton, A.J., Lübcke, P., 2013. Applying UV cameras for SO<sub>2</sub> detection to distant or optically thick volcanic plumes. *J. Volcanol. Geotherm. Res.* 262, 80–89. <https://doi.org/10.1016/j.jvolgeores.2013.06.009>

- Klein, A., Lübcke, P., Bobrowski, N., Kuhn, J., Platt, U., 2017. Plume propagation direction determination with SO<sub>2</sub> cameras. *Atmos. Meas. Tech* 10, 979–987. <https://doi.org/10.5194/amt-10-979-2017>
- Kremers, S., Wassermann, J., Meier, K., Pelties, C., van Driel, M., Vasseur, J., Hort, M., 2013. Inverting the source mechanism of Strombolian explosions at Mt. Yasur, Vanuatu, using a multi-parameter dataset. *J. Volcanol. Geotherm. Res.* 262, 104–122. <https://doi.org/10.1016/j.jvolgeores.2013.06.007>
- Laiolo, M., Massimetti, F., Cigolini, C., Ripepe, M., Coppola, D., 2018. Long-term eruptive trends from space-based thermal and SO<sub>2</sub> emissions: a comparative analysis of Stromboli, Batu Tara and Tinakula volcanoes. *Bull. Volcanol.* 80, 1–19. <https://doi.org/10.1007/s00445-018-1242-0>
- Liu, E.J., Wood, K., Mason, E., Edmonds, M., Aiuppa, A., Giudice, G., Bitetto, M., Francofonte, V., Burrow, S., Richardson, T., Watson, M., Pering, T.D., Wilkes, T.C., McGonigle, A.J.S., Velasquez, G., Melgarejo, C., Bucarey, C., 2019. Dynamics of Outgassing and Plume Transport Revealed by Proximal Unmanned Aerial System (UAS) Measurements at Volcán Villarrica, Chile. *Geochemistry, Geophys. Geosystems* 20, 730–750. <https://doi.org/10.1029/2018GC007692>
- Lübcke, P., Bobrowski, N., Illing, S., Kern, C., Alvarez Nieves, J.M., Vogel, L., Zielcke, J., Delgado Granados, H., Platt, U., 2013. On the absolute calibration of SO<sub>2</sub> cameras. *Atmos. Meas. Tech.* 6, 677–696. <https://doi.org/10.5194/amt-6-677-2013>
- Marchetti, E., Ripepe, M., Harris, A.J.L., Delle Donne, D., 2009. Tracing the differences between Vulcanian and Strombolian explosions using infrasonic and thermal radiation energy. *Earth Planet. Sci. Lett.* 279, 273–281. <https://doi.org/10.1016/j.epsl.2009.01.004>
- McGonigle, A.J.S., Aiuppa, A., Ripepe, M., Kantzas, E.P., Tamburello, G., 2009. Spectroscopic capture of 1 Hz volcanic SO<sub>2</sub> fluxes and integration with volcano geophysical data. *Geophys. Res. Lett.* 36, 1–5. <https://doi.org/10.1029/2009GL040494>
- McGonigle, A.J.S., Hilton, D.R., Fischer, T.P., Oppenheimer, C., 2005. Plume velocity determination for volcanic SO<sub>2</sub> flux measurements. *Geophys. Res. Lett.* 32, 1–4. <https://doi.org/10.1029/2005GL022470>
- McGonigle, A.J.S., Pering, T.D., Wilkes, T.C., Tamburello, G., D'Aleo, R., Bitetto, M., Aiuppa, A., Willmott, J.R., 2017. Ultraviolet Imaging of Volcanic Plumes: A New Paradigm in Volcanology. *Geosciences* 7, 68. <https://doi.org/10.3390/geosciences7030068>
- Meier, K., Hort, M., Wassermann, J., Garaebiti, E., 2016. Strombolian surface activity regimes at Yasur volcano, Vanuatu, as observed by Doppler radar, infrared camera and infrasound. *J. Volcanol. Geotherm. Res.* 322, 184–195. <https://doi.org/10.1016/j.jvolgeores.2015.07.038>
- Métrich, N., Allard, P., Aiuppa, A., Bani, P., Bertagnini, A., Shinohara, H., Parello, F., Di Muro, A., Garaebiti, E., Belhadj, O., Massare, D., 2011. Magma and Volatile Supply to Post-collapse Volcanism and Block Resurgence in Siwi Caldera (Tanna Island, Vanuatu Arc). *J. Petrol.* 52, 1077–1105. <https://doi.org/10.1093/petrology/egr019>
- Mori, T., Burton, M., 2009. Quantification of the gas mass emitted during single explosions on Stromboli with the SO<sub>2</sub> imaging camera. *J. Volcanol. Geotherm. Res.* 188, 395–400. <https://doi.org/10.1016/j.jvolgeores.2009.10.005>
- Mori, T., Burton, M., 2006. The SO<sub>2</sub> camera: A simple, fast and cheap method for ground-based imaging of SO<sub>2</sub> in volcanic plumes. *Geophys. Res. Lett.* 33, L24804. <https://doi.org/10.1029/2006GL027916>
- Oppenheimer, C., Bani, P., Calkins, J.A., Burton, M.R., Sawyer, G.M., 2006. Rapid FTIR sensing of volcanic gases released by Strombolian explosions at Yasur volcano, Vanuatu. *Appl. Phys. B* 85, 453–460. <https://doi.org/10.1007/s00340-006-2353-4>

- Oppenheimer, C., Lomakina, A.S., Kyle, P.R., Kingsbury, N.G., Boichu, M., 2009. Pulsatory magma supply to a phonolite lava lake. *Earth Planet. Sci. Lett.* 284, 392–398. <https://doi.org/10.1016/j.epsl.2009.04.043>
- Parfitt, E.A., 2004. A discussion of the mechanisms of explosive basaltic eruptions. *J. Volcanol. Geotherm. Res.* 134, 77–107. <https://doi.org/10.1016/j.jvolgeores.2004.01.002>
- Patrick, M.R., Harris, A.J.L., Ripepe, M., Dehn, J., Rothery, D.A., Calvari, S., 2007. Strombolian explosive styles and source conditions: Insights from thermal (FLIR) video. *Bull. Volcanol.* 69, 769–784. <https://doi.org/10.1007/s00445-006-0107-0>
- Pering, T.D., Ilanko, T., Liu, E.J., 2019a. Periodicity in Volcanic Gas Plumes: A Review and Analysis. *Geosci.* 2019, Vol. 9, Page 394 9, 394. <https://doi.org/10.3390/GEOSCIENCES9090394>
- Pering, T.D., Ilanko, T., Wilkes, T.C., England, R.A., Silcock, S.R., Stanger, L.R., Willmott, J.R., Bryant, R.G., McGonigle, A.J.S., 2019b. A Rapidly Convecting Lava Lake at Masaya Volcano, Nicaragua. *Front. Earth Sci.* 6, 241. <https://doi.org/10.3389/feart.2018.00241>
- Pering, T.D., McGonigle, A.J.S., 2018. Combining Spherical-Cap and Taylor Bubble Fluid Dynamics with Plume Measurements to Characterize Basaltic Degassing. *Geosciences* 8, 42. <https://doi.org/10.3390/geosciences8020042>
- Pering, T.D., McGonigle, A.J.S., James, M.R., Capponi, A., Lane, S.J., Tamburello, G., Aiuppa, A., 2017. The dynamics of slug trains in volcanic conduits: Evidence for expansion driven slug coalescence. *J. Volcanol. Geotherm. Res.* 348, 26–35. <https://doi.org/10.1016/J.JVOLGEORES.2017.10.009>
- Pering, T.D., McGonigle, A.J.S., James, M.R., Tamburello, G., Aiuppa, A., Delle Donne, D., Ripepe, M., 2016. Conduit dynamics and post-explosion degassing on Stromboli: a combined UV camera and numerical modelling treatment. *Geophys. Res. Lett.* <https://doi.org/10.1002/2016GL069001>
- Pering, T. D., McGonigle, A.J.S., James, M.R., Tamburello, G., Aiuppa, A., Delle Donne, D., Ripepe, M., 2016. Conduit dynamics and post explosion degassing on Stromboli: A combined UV camera and numerical modeling treatment. *Geophys. Res. Lett.* 43, 5009–5016. <https://doi.org/10.1002/2016GL069001>
- Pering, T.D., Tamburello, G., McGonigle, A.J.S., Aiuppa, A., Cannata, A., Giudice, G., Patanè, D., 2014. High time resolution fluctuations in volcanic carbon dioxide degassing from Mount Etna. *J. Volcanol. Geotherm. Res.* 270, 115–121. <https://doi.org/10.1016/j.jvolgeores.2013.11.014>
- Pering, T.D., Tamburello, G., McGonigle, A.J.S., Aiuppa, A., James, M.R., Lane, S.J., Scotto, M., Cannata, A., Patanè, D., 2015. Dynamics of mild strombolian activity on Mt. Etna. *J. Volcanol. Geotherm. Res.* 300, 103–111. <https://doi.org/10.1016/j.jvolgeores.2014.12.013>
- Peters, N., Hoffmann, A., Barnie, T., Herzog, M., Oppenheimer, C., 2015. Use of motion estimation algorithms for improved flux measurements using SO<sub>2</sub> cameras. *J. Volcanol. Geotherm. Res.* 300, 58–69. <https://doi.org/10.1016/j.jvolgeores.2014.08.031>
- Peters, N., Oppenheimer, C., 2018. Plumetrack: Flux calculation software for UV cameras. *Comput. Geosci.* 118, 86–90. <https://doi.org/10.1016/j.cageo.2018.05.014>
- Platt, U., Lübcke, P., Kuhn, J., Bobrowski, N., Prata, F., Burton, M., Kern, C., 2015. Quantitative imaging of volcanic plumes — Results, needs, and future trends. *J. Volcanol. Geotherm. Res.* 300, 7–21. <https://doi.org/10.1016/j.jvolgeores.2014.10.006>
- Polacci, M., Baker, D.R.D., La Rue, Alexandra, Mancini, L., Allard, P., Rue, A La, Mancini, L., 2012. Degassing behaviour of vesiculated basaltic magmas: an example from Ambrym volcano, Vanuatu Arc 233–234, 55–64. <https://doi.org/10.1016/J.JVOLGEORES.2012.04.019>

- Ripepe, M., Harris, A.J.L., Carniel, R., 2002. Thermal, seismic and infrasonic evidences of variable degassing rates at Stromboli volcano. *J. Volcanol. Geotherm. Res.* 118, 285–297. [https://doi.org/10.1016/S0377-0273\(02\)00298-6](https://doi.org/10.1016/S0377-0273(02)00298-6)
- Ripepe, M., Harris, A.J.L., Marchetti, E., 2005. Coupled thermal oscillations in explosive activity at different craters of Stromboli volcano. *Geophys. Res. Lett.* 32, 1–4. <https://doi.org/10.1029/2005GL022711>
- Ripepe, M., Marchetti, E., 2002. Array tracking of infrasonic sources at Stromboli volcano. *Geophys. Res. Lett.* 29, 33-1-33–4. <https://doi.org/10.1029/2002gl015452>
- Salvatore, V., Cigala, V., Taddeucci, J., Arciniega-Ceballos, A., Peña Fernández, J.J., Alatorre-Ibargüengoitia, M.A., Gaudin, D., Palladino, D.M., Kueppers, U., Scarlato, P., 2020. Gas-Pyroclast Motions in Volcanic Conduits During Strombolian Eruptions, in Light of Shock Tube Experiments. *J. Geophys. Res. Solid Earth* 125. <https://doi.org/10.1029/2019JB019182>
- Salvatore, V., Silleni, A., Corneli, D., Taddeucci, J., Palladino, D.M., Sottili, G., Bernini, D., Andronico, D., Cristaldi, A., 2018. Parameterizing multi-vent activity at Stromboli Volcano (Aeolian Islands, Italy). *Bull. Volcanol.* 80, 64. <https://doi.org/10.1007/s00445-018-1239-8>
- Seyfried, R., Freundt, A., 2000. Experiments on conduit flow and eruption behavior of basaltic volcanic eruptions. *J. Geophys. Res.* 105, 23727. <https://doi.org/10.1029/2000JB900096>
- Shinohara, H., Ohminato, T., Takeo, M., Tsuji, H., 2015. Monitoring of volcanic gas composition at Asama volcano, Japan, during 2004–2014. *J. Volcanol.*
- Shinohara, H., Witter, J.B., 2005. Volcanic gases emitted during mild Strombolian activity of Villarrica volcano, Chile. *Geophys. Res. Lett.* 32, L20308. <https://doi.org/10.1029/2005GL024131>
- Simons, B.C., Jolly, A.D., Eccles, J.D., Cronin, S.J., 2020. Spatiotemporal Relationships between Two Closely-spaced Strombolian-style Vents, Yasur, Vanuatu. *Geophys. Res. Lett.* 47. <https://doi.org/10.1029/2019GL085687>
- Spina, L., Taddeucci, J., Cannata, A., Gresta, S., Lodato, L., Privitera, E., Scarlato, P., Gaeta, M., Gaudin, D., Palladino, D.M., 2016. “Explosive volcanic activity at Mt. Yasur: A characterization of the acoustic events (9–12th July 2011).” *J. Volcanol. Geotherm. Res.* 322, 175–183. <https://doi.org/10.1016/j.jvolgeores.2015.07.027>
- Spina, A. La, Burton, M.R., Harig, R., Mure, F., Rusch, P., Jordan, M., Caltabiano, T., 2013. New insights into volcanic processes at Stromboli from Cerberus , a remote-controlled open-path FTIR scanner system. *J. Volcanol. Geotherm. Res.* 249, 66–76. <https://doi.org/10.1016/j.jvolgeores.2012.09.004>
- Suckale, J., Keller, T., Cashman, K. V., Persson, P.O., 2016. Flow-to-fracture transition in a volcanic mush plug may govern normal eruptions at Stromboli. *Geophys. Res. Lett.* 43, 12,071–12,081. <https://doi.org/10.1002/2016GL071501>
- Suckale, J, Keller, T., Cashman, K. V, Persson, P.-O., 2016. Flow-to-fracture transition in a volcanic mush plug may govern normal eruptions at Stromboli. *Geophys. Res. Lett.* 43, 12071–12081. <https://doi.org/10.1002/2016GL071501>
- Sweeney, D., Kyle, P.R., Oppenheimer, C., 2008. Sulfur dioxide emissions and degassing behavior of Erebus volcano, Antarctica. *J. Volcanol. Geotherm. Res.* 177, 725–733. <https://doi.org/10.1016/j.jvolgeores.2008.01.024>
- Szramek, L., Gardner, J.E., Larsen, J., 2006. Degassing and microlite crystallization of basaltic andesite magma erupting at Arenal Volcano, Costa Rica. *J. Volcanol. Geotherm. Res.* 157, 182–201. <https://doi.org/10.1016/j.jvolgeores.2006.03.039>
- Taddeucci, J., Edmonds, M., Houghton, B., James, M.R., Vergnolle, S., 2015. Hawaiian and Strombolian Eruptions, in: *The Encyclopedia of Volcanoes*. Elsevier, pp. 485–503.



- <https://doi.org/10.1016/b978-0-12-385938-9.00027-4>
- Taddeucci, J., Scarlato, P., Capponi, A., Del Bello, E., Cimarelli, C., Palladino, D.M., Kueppers, U., Bello, E. Del, Cimarelli, C., Palladino, D.M., Kueppers, U., 2012. High-speed imaging of Strombolian explosions: The ejection velocity of pyroclasts. *Geophys. Res. Lett.* 39, 1–6. <https://doi.org/10.1029/2011GL050404>
- Tamburello, G., Aiuppa, A., Kantzas, E.P., Mcgonigle, A.J.. S., Ripepe, M., 2012. Passive vs . active degassing modes at an open-vent volcano ( Stromboli , Italy ). *Earth Planet. Sci. Lett.* 359–360, 106–116. <https://doi.org/10.1016/j.epsl.2012.09.050>
- Tamburello, G., Aiuppa, A., McGonigle, A.J.S., Allard, P., Cannata, A., Giudice, G., Kantzas, E.P., Pering, T.D., 2013. Periodic volcanic degassing behavior: The Mount Etna example. *Geophys. Res. Lett.* 40, 4818–4822. <https://doi.org/10.1002/grl.50924>
- Thielicke, W., 2014. The flapping flight of birds : analysis and application. [S.n.].
- Thielicke, W., Stamhuis, E.J., 2014. PIVlab – Towards User-friendly, Affordable and Accurate Digital Particle Image Velocimetry in MATLAB. *J. Open Res. Softw.* 2. <https://doi.org/10.5334/jors.bl>
- Vergnolle, S., Boichu, M., Caplan-Auerbach, J., 2004. Acoustic measurements of the 1999 basaltic eruption of Shishaldin volcano, Alaska 1. Origin of Strombolian activity. *J. Volcanol. Geotherm. Res.* 137, 109–134. <https://doi.org/10.1016/j.jvolgeores.2004.05.003>
- Vergnolle, S., Jaupart, C., 1986. Separated two-phase flow and basaltic eruptions. *J. Geophys. Res. Solid Earth* 91, 12842–12860. <https://doi.org/10.1029/JB091iB12p12842>
- Wilkes, T., McGonigle, A., Pering, T., Taggart, A., White, B., Bryant, R., Willmott, J., Wilkes, T.C., McGonigle, A.J.S., Pering, T.D., Taggart, A.J., White, B.S., Bryant, R.G., Willmott, J.R., 2016. Ultraviolet Imaging with Low Cost Smartphone Sensors: Development and Application of a Raspberry Pi-Based UV Camera. *Sensors* 16, 1649. <https://doi.org/10.3390/s16101649>
- Wilkes, T., Pering, T., McGonigle, A., Tamburello, G., Willmott, J., Wilkes, T.C., Pering, T.D., McGonigle, A.J.S., Tamburello, G., Willmott, J.R., 2017. A Low-Cost Smartphone Sensor-Based UV Camera for Volcanic SO<sub>2</sub> Emission Measurements. *Remote Sens.* 9, 27. <https://doi.org/10.3390/rs9010027>
- Williams-Jones, G., Horton, K.A., Elias, T., Garbeil, H., Mougini-Mark, P.J., Sutton, A.J., Harris, A.J.L., 2006. Accurately measuring volcanic plume velocity with multiple UV spectrometers. *Bull. Volcanol.* 68, 328–332. <https://doi.org/10.1007/s00445-005-0013-x>
- Woitischek, J., Woods, A.W., Edmonds, M., Oppenheimer, C., Aiuppa, A., Pering, T.D., Ilanko, T., D'Aleo, R., Garaebiti, E., 2020. Strombolian eruptions and dynamics of magma degassing at Yasur Volcano (Vanuatu). *J. Volcanol. Geotherm. Res.*